第 49 卷 第 16 期/2022 年 8 月/中国激光 研究论文

中国激光

超疏水低黏附自清洁类蝶鳞片仿生结构的激光构筑与力学机理

李晶[1*]，丛居平[1]，郭楠[1]，杜新[1]，张景然[1]，杜锋[2]

[1]长春理工大学机电工程学院，吉林 长春 130022；

[2]陆军装甲兵学院士官学校基础部，吉林 长春 130117

摘要 受自然界素饰蛱蝶翅膀鳞片表面结构的启发，本研究团队建立仿生结构模型，利用激光烧蚀技术在粗化铝合金表面构建了一种具有超疏水、低黏附、自清洁性能的仿生网格状多级结构。采用扫描电子显微镜(SEM)、X 射线光电子能谱仪(XPS)、光学接触角测量仪和高速成像等设备对材料表面进行了表征分析，结果表明：喷砂粗化结合激光烧蚀可以形成类蛱蝶鳞片网格状多级结构，该结构具有复杂的形态和复合尺度特征，其表面具有超疏水性能，静态接触角可达到 162.6°，滚动角小于 5°；液滴弹跳试验和自清洁性能试验结果表明，该仿生结构表面具有良好的低黏附力和自清洁性能，在脱附、减阻、自清洁等领域具有一定的应用潜力。

关键词 激光技术；微观结构制造；超疏水表面；自清洁；低黏附；仿生结构

中图分类号 TN249 **文献标志码** A **DOI**：10.3788/CJL202249.1602009

1 引 言

超疏水[1-4]表面具有耐腐蚀[5]、抗结冰[6-7]、防雾[8-9]、防污[10]等优异特性，在机械制造、工业生产、电子信息等领域具有广阔的应用前景。然而，在使用过程中，超疏水材料因表面极易受到粉尘等污染物影响而出现性能下降。因此，研制具有自清洁[11-13]、低黏附[14-15]性能的超疏水表面非常有必要。目前，这种复合功能表面主要通过构筑微/纳米结构结合低表面能化学物质修饰实现，如：徐凯乐等[16]通过水热法在不锈钢金属网基底上生长出具有纳米柱状结构的氧化锌晶体，然后用低表面能长链硅烷对金属网进行表面改性，制备出了具有超疏水、低黏附性能的金属网材料；钱晨等[17]采用电沉积方法在碳钢表面沉积镍镀层，然后结合硬脂酸修饰获得了接触角为 160.99°的超疏水、自清洁碳钢表面；万闪等[18]采用 $FeCl_3$/HCL 混合溶液化学刻蚀与全氟癸基三氯硅烷化学改性相结合，在 AA6061 铝合金表面构筑了具有自清洁性能的超疏水表面。以上加工方法在很大程度上提升了金属表面的疏水性能，但其需要化学修饰手段，因而限制了这些方法的推广应用。因此，摒弃化学修饰手段，采用无修饰加工手段制备金属功能表面具有重要的研究价值。激光加工方法[19-23]具有基材适用范围广、操作方便、无接触等优点，而且加工微纳结构时具有可调控性好、加工精度高的特点。钟敏霖研究团队[24]使用飞秒激光器在 T2 铜和 6061 铝合金上制备了周期性三维微米锥阵列表面结构；周培阳等[25]通过调控激光脉冲宽度，利用纳秒激光器在工业纯铜表面制备了不同微米形貌的表面结构；Li 等[26]采用纳秒光纤激光器调控参数在不锈钢表面加工出“井”形微米/纳米级沟槽/凸起结构。本课题组[27]在前期的研究中采用激光烧蚀方法于不同材料表面构筑了多种仿生微米结构，并通过调控激光加工参数，获得了具有不同效应的超疏水表面，这是本研究的重要基础。

当前，仿生研究[28-29]越来越热，聚焦前沿，解决卡脖子问题是研究人员一直追求的目标。研究发现，蝴蝶翅膀鳞片表面独特的微结构是其具有疏水自清洁性能的关键因素。本文基于相似理论，受蝴蝶翅膀鳞片结构效应的启发，采用喷砂与激光加工相结合的技术，在 7075 铝合金表面构筑了类蝴蝶翅膀的网格状多级微结构，研究了仿生网格状多级结构的超疏水性、自清洁性和黏附性。

2 试 验

2.1 材 料

试验基底材料为 7075 铝合金，使用高速电火花线

收稿日期：2021-10-12；**修回日期**：2021-11-08；**录用日期**：2021-12-06

基金项目：国家自然科学基金(51975060，51505039，51905047)、吉林省科学技术厅自然科学基金(20180101322JC)、吉林省教育厅科学技术研究项目(JJKH20210810KJ)

通信作者：*jl2015edu@163.com

切割机床将其切割成尺寸为 20 mm×10 mm×2 mm 的试样。试验过程使用的化学试剂为去离子水、乙醇(分析级)、氯化钠溶液(分析级)。

2.2 样品制备

采用 600#、800#、1000#、1500#、2000# 金相砂纸逐次打磨试样,然后进行抛光处理,之后用超声波清洗,最后烘干备用。对光滑基底试样进行喷砂处理,喷料粒径为 100～120 μm,喷砂压力为 0.50～0.60 MPa,放置角度为 80°～90°,喷砂距离为 15～20 mm,喷砂时间为 30～40 s。喷砂结束后,将试样分别放入乙醇、丙酮以及去离子水中进行超声清洗,清洗干净后烘干。使用光纤激光器在经过上述预处理的铝合金试样表面进行仿生结构的加工,激光加工功率为 10 W,激光波长为 1060 nm,光斑直径为 40 μm,脉冲持续时间为 10 μs,扫描频率为 20 kHz,扫描速度为 50 mm/s,调节激光加工间距(50,100,150,200 μm),分别在水平与垂直方向上重复进行 2 次扫描,最后将经过激光加工的试样清洗干净,进行干燥处理。

2.3 样品表征

采用 JSM-6510LA 型扫描电子显微镜(SEM)观察样品的表面形貌;利用 SPECSXR50 型 X 射线光电子能谱仪(XPS)分析样品表面的物相组成;室温(约 20 ℃)下,使用 OCA15 Pro 光学接触角测量仪测量样品表面的接触角和滚动角(使用去离子水,液滴体积为 3 μL,取三个位置的平均值);采用高速相机拍摄液滴落在样品表面的动态过程(使用去离子水,液滴体积为 15 μL,液滴高度为 30 mm)。

3 分析与讨论

3.1 表面微观特征

参考蝴蝶翅膀的独特结构建立网格状仿生模型,并使用激光加工技术在喷砂铝合金表面制备网格状凹槽结构。图 1(a-1)、(a-2)、(a-3)为蝴蝶翅膀上鳞片的微结构[30-31],鳞片表面分布着复杂的交联结构[如图 1(a-3)所示],并在其上端平行排列着由丝状物相互连接的脊状结构,如图 1(a-1)、(a-2)所示。本课题组基于这种独特的网格状结构建立了三维模型,如图 1(b)所示。模型由规则的网格状沟槽结构紧密排列,内方边长为 a_1,外方边长为 a_2,槽宽为 b,凹面槽深为 h、未烧蚀铝合金表面宽度为 a。采用喷砂与激光加工相结合的方法[如图 1(c)所示]在铝合金基底制备网格状结构。喷砂粗化表面呈微米级层片状结构,激光在粗化表面烧蚀出网格状沟槽结构。预期加工形成的复合微结构能够增大固体表面的气相占比,使仿生表面具有疏水性能。

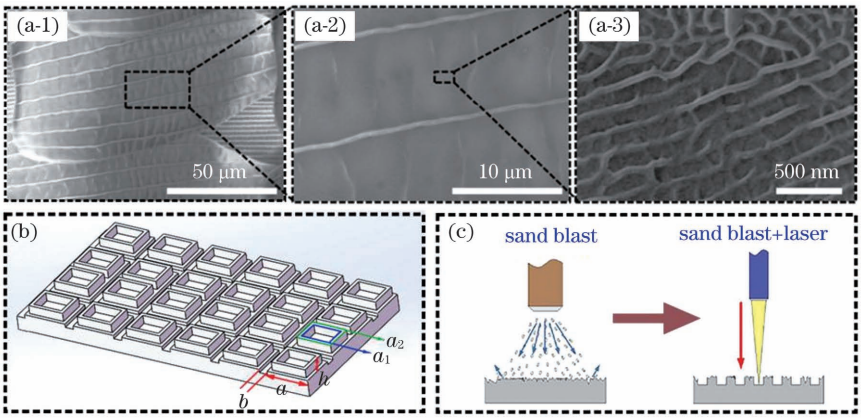

图 1 仿生结构的建立及制备过程。(a)蝴蝶翅膀的网格状结构[30];(b)仿生模型;(c)试样制备过程

Fig. 1 Design and preparation of biomimetic structure. (a) Grid structure of butterfly wings[30]; (b) biomimetic model; (c) sample preparation process

利用扫描电子显微镜对不同激光加工间距下的表面形貌进行详细分析。图 2(a-1)、(a-2)为喷砂粗化试样表面的放大图像,因不同试样表面喷砂参数设置相同,所以只放置一组图片。可以看出,喷砂粗化试样表面形成了微米级层片状结构,获得了一定的粗糙度,该结构为一级结构。图 2(b-1)、(c-1)、(d-1)、(e-1)是试样表面在激光束的高能作用下构筑而成的复杂网格结构,该结构由粗糙基底和沟槽组成,为二级结构,沟槽宽度约为 20 μm,深度约为 25 μm。由图 2(b-2)、(c-2)、(d-2)、(e-2)可知,随着激光加工间距的增加,未烧蚀的粗糙铝合金表面占比逐渐增大,金属飞溅物在网格状沟槽边缘堆积,飞溅物直径为 3～4 μm,飞溅物与交错的沟槽形成了一体化互连三级结构。为分析不同激光加工间距下试样表面微结构的高度,利用激光共聚焦显微镜(LSCM)进行观察,结果如图 2(b-3)、(c-3)、(d-3)、(e-3)所示。

3.2 表面润湿特性

3.2.1 静态接触角

为了解不同激光加工间距下制得的结构形貌对表面润湿性的影响,对仿生试样表面进行接触角测量。图 3(a)是不同激光加工间距下静态接触角(CA)的测量结果。可以看出,静态接触角随着激光加工间距的增大而减小,当激光加工间距为 50 μm 时,仿生试样表面的液滴接近球形,静态接触角可达到 162.6°,表面呈超疏水状态。在本文参数调控范围内,液滴浸入表面结构后的形态满足Cassie-Baxter状态方程。由

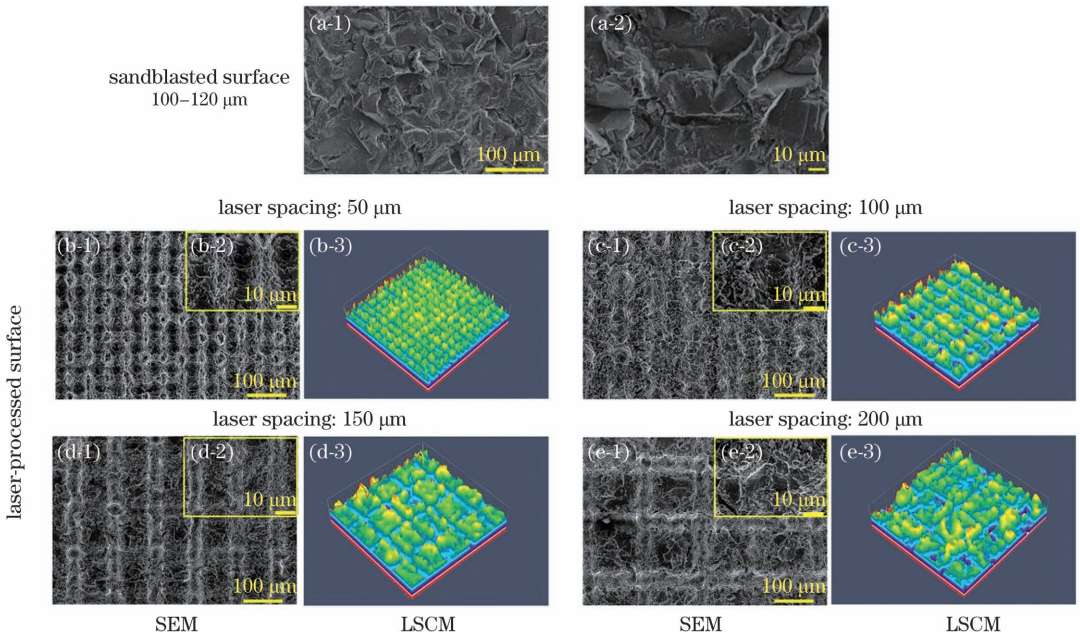

图 2 加工试样表面的微观形貌

Fig. 2 Surface morphologies of processed samples

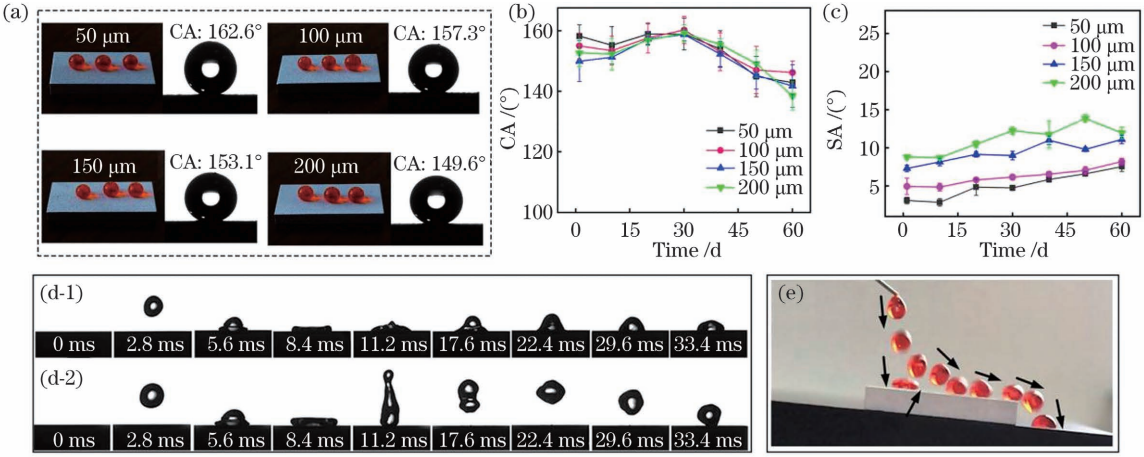

图 3 试样表面润湿性测试。(a)不同激光加工间距下表面接触角的测量结果;(b)静态接触角的稳定性;(c)滚动角的稳定性;(d)液滴的弹跳性能,(d-1)为抛光表面,(d-2)为仿生表面;(e)仿生表面黏附特性测试

Fig. 3 Wettability test of samples. (a) Contact angle (CA) measurement results for different laser processing spacing values; (b) stability of static contact angle; (c) stability of rolling angle (SA); (d) droplet bounce performance, where (d-1) represents polished sample and (d-2) represents biomimetic sample; (e) adhesion test of biomimetic specimen surface

于液滴和空气之间的接触角为 180°,因此 Cassie-Baxter 状态方程可以表示为

$$\cos\theta_{CB} = f(\cos\theta_0 + 1) - 1, \tag{1}$$

式中:f 为固-液界面所占的比例,即固-液接触面积与总面积的比值;θ_0 为光滑表面的接触角;θ_{CB} 为仿生试样表面的接触角。随着激光加工间距的增大,未烧蚀的粗糙铝合金表面占比逐渐增大,液滴逐渐浸入,固-液界面所占比例增大,因此接触角减小[32]。

图 3(b)是将仿生试样放置不同时间后的稳定性测试结果。可以看出,静态接触角在前 30 天整体呈增大趋势,在第 30 天时静态接触角达到最大值,随后逐渐下降直至试验结束。前 30 天,空气中的有机物会与铝合金试样表面结合,加快润湿性转变;放置过长时间后,试样表面不再进一步氧化,空气和水分子无法与新的 Al_2O_3 结合,而是吸附在试样表面,因此接触角减小[33-34]。在整个试验过程中,静态接触角在 150°附近上下波动,这表明仿生试样表面保持着良好的超疏水特性。

3.2.2 动态接触角

对不同激光加工间距下的仿生试样表面进行动态接触角测试,测试结果如表 1 所示,各表面均获得了接触角大于 150°的超疏水特性,且接触角滞后小于 7°,50 μm 激光加工间距下的表面表现出了最优的疏水特性。图 3(c)是滚动角(SA)稳定性测试结果。可以看出,仿生试样的滚动角变化不大,说明长时间放置后试样表面依旧能维持低黏附性能。使用高速相机拍摄了液滴落在抛光/仿生试样表面的过程,结果如图 3(d)所示。图 3(d-1)展示了液滴落在抛光试样表面扩散

收缩不回弹的现象，而图 3(d-2)则展示了液滴落在仿生试样表面扩散收缩并回弹上升至一定高度后才落下的过程，而且液滴在回弹过程中受仿生试样表面微结构黏附力的影响而被拉长。液滴下滑试验和弹跳试验结果表明，液滴在激光加工间距为 50 μm 的试样表面具有最佳的低黏附性和良好的主动滚动倾向。为了更直观地观测仿生试样表面的低黏附性能，选择图 3(e)所示的方案，将试样置于倾角为 5°的平台上，在试样表面垂直高度为 20 mm 处滴落液滴至试样表面。可以发现液滴循环反弹，最终弹出试样表面。

表 1 不同激光加工间距下液滴的动态接触特性

Table 1 Dynamic contact performance of a water droplet on aluminum alloy surfaces fabricated with different laser processing spacing values

Laser processing spacing /μm	Advance angle /(°)	Receding angle /(°)	Contact angle hysteresis /(°)
50	164.4	161.2	3.2
100	159.7	155.2	4.5
150	156.3	150.1	6.2
200	155.1	148.2	6.9

3.3 表面的自清洁特性

选取固相粉尘和固液混合泥浆两种不同的污染物进行试样表面的污染/自清洁性能测试。图 4(a)、(b)所示为两种试样表面的除粉尘试验，即：使液滴在距离倾斜5°试样平面一定高度处垂直下落。可以看到：液滴将抛光试样表面的部分杂质不规则地去除，但是在液相的渗透下，有部分粉尘黏附在试样表面；而在仿生试样表面，滴落的液滴携带着粉尘快速离开试样表面，仿生试样展现出了良好的自清洁效果。图 4(c)、(d)展示了固液混合泥浆环境中两种试样表面的自清洁能力。可以看出：抛光试样浸入泥浆中浸泡后被污染了，而仿生试样从泥浆中离开后，表面没有泥浆残留。这说明仿生试样表现出了不润湿现象，具有优异的自清洁特性。

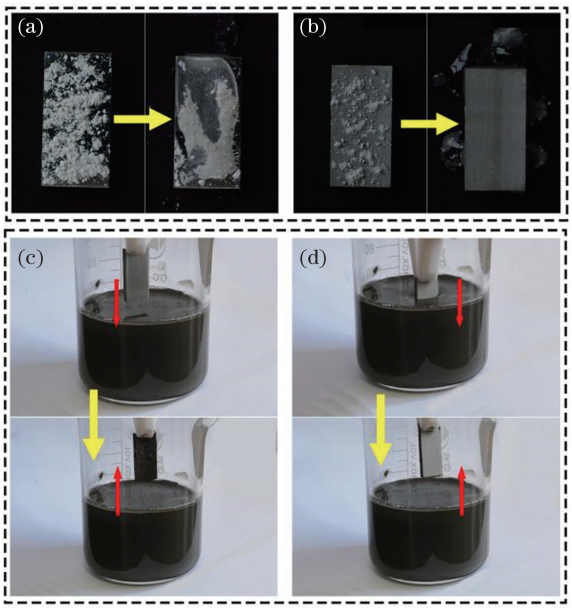

图 4 试样在不同污染环境下的污染/自清洁行为。(a)粉尘环境下的抛光试样；(b)粉尘环境下的仿生试样；(c)泥浆环境下的抛光试样；(d)泥浆环境下的仿生试样

Fig. 4 Contamination/self-cleaning behavior of samples in different pollution environments. (a) Polished sample in dust environment; (b) biomimetic sample in dust environment; (c) polished sample in mud environment; (d) biomimetic sample in mud environment

3.4 机理分析

3.4.1 表面成分

为分析激光加工前后试样表面润湿性转变的原因，对铝合金抛光试样和仿生试样表面进行了 XPS 测试分析，测试结果如图 5 所示。从图 5(a1)、(a2)可以看出，抛光试样和仿生试样表面的主要组分均为 C、O、Si、Al 和 Zn 元素，各元素峰分别位于 284，531，101，73，1021 eV 处。Si、Al 和 Zn 元素主要来自基底材料，抛光试样表面的 C 元素主要来自测试设备腔室内的污染和空气中有机化合物的吸附，此外，放置过程中试样表面的氧化也会导致 O 元素增加。为进一步分析仿生试样表面 C 元素和 O 元素的来源，将 C1s 峰分解为 284.4 eV 处的 C—C 峰、286 eV 处 C—O 峰和 288.5 eV 处的 C═O 峰，其中 C—C 为非极性基团，C—O、C═O 为极性基团，表面极性会影响材料的疏水性，即：非极性基团含量的增加对表面疏水性有一定的促进作用[26]。由图 5(b1)、(b2)可知，抛光试样和仿生试样表面 C—C 非极性基团的占比分别为 80.7% 和 87.9%。这表明激光加工试样放置在空气中吸附的化合物主要由非极性化合物组成，且相比抛光试样表面非极性化合物的含量有所增加，因此表面疏水性得到了大幅度提高。对 O 元素进行分峰，结果如图 5(c)所示。可以看出，抛光试样和仿生试样表面 Al_2O_3 含量的变化不大，说明这两种试样表面均可以形成一层稳定的氧化膜。空气中的水分子吸附在 Al_2O_3 表面引起表面羟基化，羟基与空气中的有机物结合会加快润湿性转变，进而降低表面的润湿性能[35]。

3.4.2 力学机理

为了更好地理解仿生试样表面的低黏附行为，接下来详细分析黏附力的作用机理。图 6 为液滴在仿生试样表面的示意图。黏附力是由液滴-固体界面相互作用产生的[36]，其表达式为

$$F_{ad}=kIA, \tag{2}$$

式中：F_{ad} 为黏附力；k 为常数；A 为液滴-固体界面的接触面积；I 是与试样表面化学性质有关的参数。本次试验在保持激光加工参数一致的条件下，通过调节激光加工间距获得粗糙结构表面，试样在激光烧蚀过程中的氧化性以及加工后放置在空气中形成化学键的能力一样，试样表面的化学性质相同，因此黏附力与液

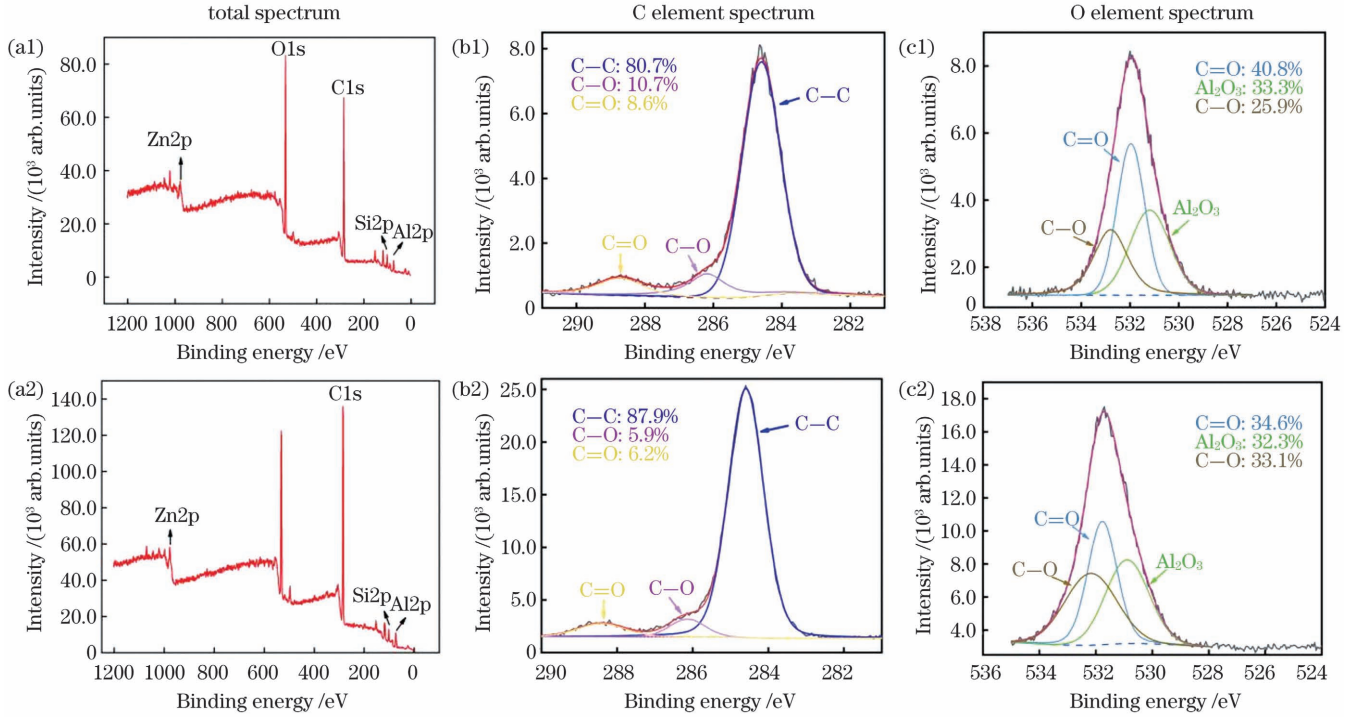

图 5 试样表面的 XPS 测试谱图。(a1)～(c1)抛光试样;(a2)～(c2)仿生试样

Fig. 5 XPS test spectra of samples surfaces. (a1)-(c1) Polished sample; (a2)-(c2) biomimetic sample

滴-固体界面接触面积 A 成正比,即

$$F_{ad} \propto A 。 \tag{3}$$

液滴-固体界面的接触面积包括沟槽结构中的凸起面积 $a_1^2-a_2^2$ 与未被激光烧蚀区域面积 a_2^2,如图 1(b)所示。一部分液滴覆盖在沟槽结构凸起表面,另一部分则随未被激光烧蚀区域面积的增加逐渐浸入结构内,使结构内部的空气大幅减少。因此,随激光加工间距的增加,液滴与凸起表面、未烧蚀区域的接触面积均增大,当激光加工间距为 50 μm 时,仿生试样表面固-液界面所占比例最小,黏附力最小,液滴在仿生试样表面具有良好的低黏附性能。当液滴在倾斜仿生试样表面时[如图 6(b)所示],液滴-固体界面变为超疏水复合界面,即液滴与仿生试样表面之间除了由液滴与固体界面的黏附力 $F_{s\text{-}ad}$ 以外,还有一个额外的液滴在沟槽内部的黏附力 $F_{g\text{-}ad}$,以往的 Furmidge 方程[如式(4)所示]并不适用。Furmidge 方程的表达式为

$$\frac{F_{ad}}{W_s}=\frac{\rho V g \sin\alpha}{W_s}=\gamma_{LV}(\cos\theta_R-\cos\theta_A), \tag{4}$$

式中:W_s 为液滴在固体界面上的宽度;ρ 为液体的密度;g 为重力加速度;V 为液滴的体积;α 为固定试样倾斜放置时与水平面的夹角;γ_{LV} 为液滴的表面张力;θ_R 为液滴在固体表面的后退接触角;θ_A 为液滴在固体表面的前进接触角。假设 $F_{s\text{-}ad}$ 和 $F_{g\text{-}ad}$ 这两种黏附力相互独立,则液滴从仿生试样表面滑落时的黏附力 F_{ad}[37]可以表示为

$$\begin{aligned}F_{ad}&=F_{s\text{-}ad}+F_{g\text{-}ad}=\\&(W_s-W_g)\gamma_{LV}(\cos\theta_{sR}-\cos\theta_{sA})+\\&W_g\gamma_{LV}(\cos\theta_{gR}-\cos\theta_{gA}),\end{aligned} \tag{5}$$

式中:$F_{s\text{-}ad}$ 为液滴与固体界面的黏附力;$F_{g\text{-}ad}$ 为液滴与凹槽内部的黏附力;W_g 为液滴在凹槽结构中的宽度;θ_{sR} 为液滴在固体表面的后退接触角;θ_{sA} 为液滴在固体表面的前进接触角;θ_{gR} 为液滴在凹槽结构中的后退接触角;θ_{gA} 液滴在凹槽结构中的前进接触角。后退接触角与前进接触角的差值为滚动角。当激光加工参数保持不变时,不同激光加工间距下的凹槽宽度一致,液滴在凹槽结构中的宽度 W_g 不变;随着激光加工间距增大,液滴在固体表面的宽度 W_s 增大,滚动角增大,黏附力提高。

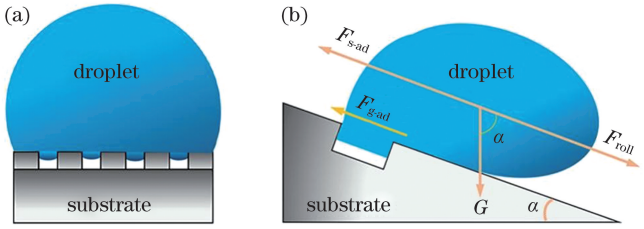

图 6 液滴在仿生试样表面的示意图。(a)液滴水平放置在表面时的接触示意图;(b)液滴放置在倾斜表面时的黏附力分析

Fig. 6 Schematics of droplet on biomimetic sample surface. (a) Surface contact diagram of droplet placed horizontally; (b) adhesion analysis diagram of droplet placed on a tilted surface

4 结 论

本课题组以喷砂粗化铝合金表面为基底,采用激光烧蚀方法构筑了仿蝴蝶翅膀鳞片表面网格状多级结构,获得了具有超疏水、低黏附和自清洁性能的多功能

表面；研究了所制备的不规则多级尺度粗糙结构对表面性能的影响。结果发现，恰当的多级结构特征（激光烧蚀线间距为 50 μm 时构筑的多级结构的静态接触角为 162.6°，滚动角小于 5°）能够捕获更多的空气，使空气进入表面结构，阻碍液滴进入结构空隙，形成 Cassie 模型下的“气垫”效应，实现超疏水特性。

本文分析了液滴在制备表面的弹跳行为和倾斜（平面倾斜角为 5°）滑动现象，结果发现激光烧蚀仿生表面具有优异的低黏附性能，液滴能快速弹跳并滑移离开表面。采用灰尘和泥浆模拟环境污染表面，结果发现：当以 5°的倾斜角放置仿生样品时，落在表面上的液滴在自身重力作用下沿着倾斜方向滚动，同时除去附着在样品表面的粉尘杂质，液滴没有润湿表面；将样品浸入自制泥浆再取出后，样品表面保持清洁，具有非常好的不润湿性和自清洁效应。对倾斜试样表面的液滴进行力学分析，验证了在 50 μm 激光烧蚀线间距下制备的结构表面与液滴界面间具有最小的黏附力，液滴最易发生滚动并带走污染物，与试验结果相符。本研究证明了通过构筑多尺度微结构能够直接实现铝合金表面集超疏水性、低黏附性和自清洁性于一体。

参 考 文 献

[1] 陈峒霖, 毛江维, 陈招弟, 等. 激光加工制备仿芦苇叶结构的超疏水表面[J]. 科学通报, 2019, 64(12): 1303-1308.
Chen T L, Mao J W, Chen C D, et al. Fabrication of bionic reed leaf superhydrophobic surface by laser processing[J]. Chinese Science Bulletin, 2019, 64(12): 1303-1308.

[2] Marmur A, Kojevnikova S. Super-hydrophobic surfaces: methodological considerations for physical design[J]. Journal of Colloid and Interface Science, 2020, 568: 148-154.

[3] Wang J N, Liu Y Q, Zhang Y L, et al. Wearable superhydrophobic elastomer skin with switchable wettability[J]. Advanced Functional Materials, 2018, 28(23): 1800625.

[4] 丁雅玉, 苏亚辉, 陈亮. 纳秒激光加工(超)疏水/(超)亲水铝膜的润湿性和雾水收集实验研究[J]. 激光与光电子学进展, 2020, 57(11): 111412.
Ding Y Y, Su Y H, Chen L. Experimentally investigating wettability and fog collection characteristics of (super) hydrophobic/(super) hydrophilic aluminum membranes processed by nanosecond laser[J]. Laser & Optoelectronics Progress, 2020, 57(11): 111412.

[5] Li J, Lin O C, Cheng C, et al. Fabrication of a Ni/SiC composite coating on steel surface with excellent corrosion inhibition performance[J]. Journal of Materials Processing Technology, 2021, 290: 116987.

[6] Qiu C, Li M, Chen S X. Anti-icing characteristics of PTFE super hydrophobic coating on titanium alloy surface[J]. Journal of Alloys and Compounds, 2021, 860: 157907.

[7] Wei D S, Wang J G, Li S Y, et al. Novel corrosion-resistant behavior and mechanism of a biomimetic surface with switchable wettability on Mg alloy[J]. Chemical Engineering Journal, 2021, 425: 130450.

[8] 富慧中, 西鹏, 杨龙, 等. 具有高效防雾与光能转换功能的聚对苯二甲酸乙二醇酯复合膜的制备与性能[J]. 高分子材料科学与工程, 2020, 36(11): 145-151.
Fu H Z, Xi P, Yang L, et al. Preparation and properties of polyethylene terephthalate composite film with efficient anti-fog and light energy conversion functions[J]. Polymer Materials Science & Engineering, 2020, 36(11): 145-151.

[9] Han Z W, Mu Z Z, Li B, et al. Active antifogging property of monolayer SiO_2 film with bioinspired multiscale hierarchical pagoda structures[J]. ACS Nano, 2016, 10(9): 8591-8602.

[10] Wang Z H, Yuan L, Liang G Z, et al. Mechanically durable and self-healing super-hydrophobic coating with hierarchically structured KH570 modified SiO_2-decorated aligned carbon nanotube bundles[J]. Chemical Engineering Journal, 2021, 408: 127263.

[11] Chen B B, Dong Z, Jia Y H, et al. Sepiolite-based superamphiphobic coating with excellent robustness, chemical stability and self-cleaning performance[J]. Progress in Organic Coatings, 2021, 157: 106297.

[12] Zhao W R, Xiao L, He X Y, et al. Moth-eye-inspired texturing surfaces enabled self-cleaning aluminum to achieve photothermal anti-icing[J]. Optics & Laser Technology, 2021, 141: 107115.

[13] Zhang X, Dong Y Y, Pan F, et al. Electrostatic self-assembly construction of 2D MoS_2 wrapped hollow Fe_3O_4 nanoflowers@1D carbon tube hybrids for self-cleaning high-performance microwave absorbers[J]. Carbon, 2021, 177: 332-343.

[14] Laroche A, Bottone D, Seeger S, et al. Silicone nanofilaments grown on aircraft alloys for low ice adhesion[J]. Surface and Coatings Technology, 2021, 410: 126971.

[15] Kujawa J, Al-Gharabli S, Wrzeszcz G, et al. Physicochemical and magnetic properties of functionalized lanthanide oxides with enhanced hydrophobicity[J]. Applied Surface Science, 2021, 542: 148563.

[16] 徐凯乐, 付超, 徐梦亚, 等. 低粘附超疏水金属网的制备及在溢油清理中的应用[J]. 表面技术, 2017, 46(11): 37-46.
Xu K L, Fu C, Xu M Y, et al. Preparation of low adhesion superhydrophobic metal mesh and its application to oil spillage cleanup[J]. Surface Technology, 2017, 46(11): 37-46.

[17] 钱晨, 王华. 碳钢表面电镀 Ni-TiO_2 镀层硬脂酸修饰制备超疏水表面[J]. 表面技术, 2019, 48(8): 165-171.
Qian C, Wang H. Superhydrophobic surface prepared by stearic acid modification of Ni-TiO_2 coating on carbon steel surface[J]. Surface Technology, 2019, 48(8): 165-171.

[18] 万闪, 姜丹, 蔡光义, 等. 铝合金超疏水转化膜的制备与性能[J]. 材料工程, 2018, 46(9): 144-151.
Wan S, Jiang D, Cai G Y, et al. Preparation and properties of superhydrophobic conversion film on aluminium alloy[J]. Journal of Materials Engineering, 2018, 46(9): 144-151.

[19] 边玉成, 王宇龙, 肖轶, 等. 飞秒激光制备可控微纳米结构表面及应用研究[J]. 激光与光电子学进展, 2020, 57(11): 111406.
Bian Y C, Wang Y L, Xiao Y, et al. Controllable micro/nano structure surface fabricated by femtosecond laser and its applications[J]. Laser & Optoelectronics Progress, 2020, 57(11): 111406.

[20] Liang L S, Lu L S, Xing D, et al. Preparation of superhydrophobic and anti-resin-adhesive surfaces with micro/nanoscale structures on high-speed steel via laser processing[J]. Surface and Coatings Technology, 2019, 357: 57-68.

[21] Yang Z, Liu X P, Tian Y L. Insights into the wettability transition of nanosecond laser ablated surface under ambient air exposure[J]. Journal of Colloid and Interface Science, 2019, 533: 268-277.

[22] Tan D Z, Wang Z, Xu B B, et al. Photonic circuits written by femtosecond laser in glass: improved fabrication and recent progress in photonic devices[J]. Advanced Photonics, 2021, 3(2): 024002.

[23] 陈亮, 刘晓东, 刘静, 等. 飞秒激光在石英玻璃表面刻蚀微槽的研究[J]. 光学学报, 2020, 40(23): 2314001.
Chen L, Liu X D, Liu J, et al. Microgroove etching with femtosecond laser on quartz glass surfaces[J]. Acta Optica Sinica, 2020, 40(23): 2314001.

[24] 潘瑞, 张红军, 钟敏霖. 三级微纳超疏水表面的超快激光复合制备及防除冰性能研究[J]. 中国激光, 2021, 48(2): 0202009.
Pan R, Zhang H J, Zhong M L. Ultrafast laser hybrid fabrication and ice-resistance performance of a triple-scale micro/

nano superhydrophobic surface[J]. Chinese Journal of Lasers, 2021, 48(2): 0202009.
[25] 周培阳, 彭耀政, 黄泽铭, 等. 纳秒激光制备的超疏水表面及其液滴冲击性能[J]. 中国激光, 2020, 47(4): 0402012.
Zhou P Y, Peng Y Z, Huang Z M, et al. Fabrication and droplet impact performance of superhydrophobic surfaces developed using nanosecond lasers[J]. Chinese Journal of Lasers, 2020, 47(4): 0402012.
[26] Li X Y, Jiang Y, Jiang Z H, et al. Improvement of corrosion resistance of H59 brass through fabricating superhydrophobic surface using laser ablation and heating treatment[J]. Corrosion Science, 2021, 180: 109186.
[27] 李晶, 赵世才, 李强, 等. 类水稻叶多尺度表面构筑与各向疏水性[J]. 科学通报, 2017, 62(16): 1766-1773.
Li J, Zhao S C, Li Q, et al. Fabrication of biomimetic multi-scale surface of rice leaf and anisotropic superhydrophobic properties[J]. Chinese Science Bulletin, 2017, 62(16): 1766-1773.
[28] Yue D C, Lin S M, Cao M T, et al. Fabrication of transparent and durable superhydrophobic polysiloxane/SiO_2 coating on the wood surface[J]. Cellulose, 2021, 28(6): 3745-3758.
[29] 文刚, 郭志光, 刘维民. 仿生超润湿材料的研究进展[J]. 中国科学: 化学, 2018, 48(12): 1531-1547.
Wen G, Guo Z G, Liu W M. Recent developments of bioinspired materials with superwettability[J]. Scientia Sinica Chimica, 2018, 48(12): 1531-1547.
[30] Lu T, Pan H, Ma J, et al. Near-infrared trigged stimulus-responsive photonic crystals with hierarchical structures[J]. ACS Applied Materials & Interfaces, 2017, 9(39): 34279-34285.
[31] 穆正知. 基于典型蝶翅的仿生功能表面设计制造及性能研究[D]. 长春: 吉林大学, 2019: 22-23.
Mu Z Z. Design, fabrication and properties of biomimetic functional surfaces based on typical butterfly wings[D]. Changchun: Jilin University, 2019: 22-23.
[32] Guo F Q, Duan S W, Wu D T, et al. Facile etching fabrication of superhydrophobic 7055 aluminum alloy surface towards chloride environment anticorrosion[J]. Corrosion Science, 2021, 182: 109262.
[33] Barthwal S, Lim S H. A durable, fluorine-free, and repairable superhydrophobic aluminum surface with hierarchical micro/nanostructures and its application for continuous oil-water separation[J]. Journal of Membrane Science, 2021, 618: 118716.
[34] Ke X, Zhou X, Hao G Z, et al. Rapid fabrication of superhydrophobic Al/Fe_2O_3 nanothermite film with excellent energy-release characteristics and long-term storage stability[J]. Applied Surface Science, 2017, 407: 137-144.
[35] Long J Y, Zhong M L, Zhang H J, et al. Superhydrophilicity to superhydrophobicity transition of picosecond laser microstructured aluminum in ambient air[J]. Journal of Colloid and Interface Science, 2015, 441: 1-9.
[36] Ou J F, Hu W H, Li C Q, et al. Tunable water adhesion on titanium oxide surfaces with different surface structures[J]. ACS Applied Materials & Interfaces, 2012, 4(11): 5737-5741.
[37] Xiang T F, Zhang M X, Li C, et al. A facile method for fabrication of superhydrophobic surface with controllable water adhesion and its applications[J]. Journal of Alloys and Compounds, 2017, 704: 170-179.

Superhydrophobic Low Adhesion Self-Cleaning Biomimetic Surfaces: Laser Construction and Mechanical Properties of Simulated Butterfly Scales

Li Jing[1*], Cong Juping[1], Guo Nan[1], Du Xin[1], Zhang Jingran[1], Du Feng[2]
[1] *School of Mechanical and Electric Engineering, Changchun University of Science and Technology, Changchun 130022, Jilin, China;*
[2] *Department of Basic, Army Academy of Armored Forces, Changchun 130117, Jilin, China*

Abstract

Objective Superhydrophobic surfaces are corrosion-resistant and have excellent anti-icing, anti-fogging, and anti-fouling properties. They have the potential for broad applications in machinery manufacturing, industrial production, electronic information, and other fields. However, while in use, the material surface is easily affected by dust and other pollutants so that its performance decreases. Therefore, it is necessary to develop superhydrophobic surfaces with self-cleaning and low adhesion properties. At present, this kind of composite functional surface is mainly realized by constructing micro-nano structures combined with low surface-energy chemical modifications. These processing methods greatly improve the hydrophobic performance of metal surfaces; however, they limit the working conditions because of the need for terminal low-energy modification conditions. Therefore, it is urgent to adopt simple and efficient methods for preparing high-performance composite metal surfaces. Laser processing methods have advantages such as a wide range of applicability, convenient operation, and non-contact implementation; moreover, they are highly adjustable and yield high processing accuracy for the micro-nano processing of materials. In this study, a biomimetic micron-scale structure was constructed on the surface of an aluminum alloy by a laser ablation method, and a superhydrophobic low viscosity self-cleaning surface was obtained by adjusting the laser processing parameters (Fig. 1).

Methods In this work, the unique structure of butterfly wings was used as the model for a biomimetic grid; the grid groove structure was prepared on the surface of a sandblasted, coarse-grained aluminum alloy by laser processing. The surface structure of the biomimetic metal sample was optimized by adjusting the laser processing spacing. The surface morphology, chemical composition, and surface wettability of the materials were characterized by scanning electron microscopy (SEM), laser scanning confocal microscopy (LSCM), X-ray photoelectron spectroscopy (XPS), optical contact angle measurements, and high-speed imaging.

Results and Discussions The results show that: (1) After coarsening by sandblasting, the surface of the specimen formed a micron-grade sheet structure. To obtain a controlled roughness, the primary structure was formed by a high-energy laser beam that transformed the sample surface into a complex grid structure composed of a coarse basement and grooves forming the secondary structure. With the increase of separation between the laser processing paths, metal spatter accumulated at the edge of the gridded groove, forming an integrated, interconnected, three-stage structure with staggered grooves (Fig. 2). (2) The experimental contact angle measurement results show that the maximum static contact angle of the biomimetic sample surface reached 162.6° when the laser processing interval was 50 μm. The hydrophobicity of the biomimetic sample surface occurs because the microstructure formed by laser processing increases the gas-phase proportion of the solid surface. The dynamic contact angle test on the surface of the biomimetic sample shows that the best rolling angle (less than 5°) was achieved when the laser machining distance was 50 μm. The droplet slide test and droplet bounce test show that the sample has good low adhesion properties (Fig. 3 and Table 1). (3) Two different pollutants, solid-phase dust and solid-liquid mixed mud, were selected for the self-cleaning tests of the sample surface, and the sample surface showed a good self-cleaning effect (Fig. 4). (4) The samples were analyzed by XPS before and after the laser processing. Comparing these results shows that the number of nonpolar groups (i.e., C—C bonds) on the surface of the biomimetic sample increased compared to the polished sample. Since the nonpolar groups play an important role in improving the hydrophobicity, these results suggest that the compounds adsorbed from the air after laser processing are mainly nonpolar compounds. Therefore, the surface hydrophobicity of the biomimetic sample is greatly improved (Fig. 5). (5) The mechanism of adhesion force was analyzed in detail by mechanical modeling, and it was found that the adhesion force was proportional to the contact area of the droplet-solid interface. When the laser processing interval was 50 μm, the contact area of the droplet-solid interface on the surface of the biomimetic sample was the smallest, and the adhesion force was the lowest (Fig. 6).

Conclusions In this study, a multi-layer grid structure similar to the scales of a butterfly wing was constructed on the surface of an aluminum alloy by laser ablation of a surface that had been previously roughened by sandblasting; a functional surface with superhydrophobicity, low adhesion, and self-cleaning properties was obtained. It appears that a surface with appropriate multistage structural characteristics can retain more air in close proximity to the surface of the aluminum alloy material surface; this "air effect" is responsible for the superhydrophobicity, low adhesion, and cleaning effect. The adhesion properties of the laser ablated biomimetic surface were studied by analyzing the bouncing behavior of droplets on different surfaces under the same conditions and by observing the sliding phenomenon as a function of inclination angle; the laser ablated surfaces have significantly lower adhesion than the polished surface. In addition, the experiment using dust and mud to simulate environmental pollution shows that when the biomimetic sample was placed at a 5° tilt angle, water droplets falling on the surface rolled along the tilt direction under the action of gravity without wetting the surface and removed the dust impurities attached to the surface. The sample was also placed into homemade mud, and the surface of the sample was found to be clean after removal, showing a very good non-wetting and self-cleaning effect. The mechanical analysis of the droplet on the surface of the inclined sample shows that, in the multistage structure with 50 μm separation between laser ablation lines, the droplet had the minimum adhesion force and could roll easily, thereby removing pollutants; this verifies that the sample has low adhesion and good self-cleaning performance. This biomimetic composite surface has the potential to contribute in the areas of desorption, drag reduction, and self-cleaning.

Key words laser technique; microstructure fabrication; superhydrophobic surface; self-cleaning; low adhesion; biomimetic structure